Calibration of a Novel Microstructural Damage Model for Wire Bonds

L. Yang, P. A. Agyakwa, and C. M. Johnson

***Abstract*—In a previous paper, a new time-domain damage-based physics model was proposed for the lifetime prediction of wire bond interconnects in power electronic modules. Unlike cycle-dependent life prediction methodologies, this model innovatively incorporates temperature- and time-dependent properties so that rate-sensitive processes associated with the bond degradation can be accurately represented. This paper presents the work on the development and calibration of the damage model by linking its core parameter, i.e., "damage," to the strain energy density, which is a physically quantifiable materials property. Isothermal uniaxial tensile data for unbonded pure aluminum wires (99.999%) have been used to develop constitutive functions, and the model has been calibrated by the derived values of the strain energy density.**

***Index Terms*—Wire bond, physics of failure, time domain, damage model.**

I. Introduction

WIRE bonds which provide electrical interconnections in power device packaging undergo thermo mechanical fatigue due to the temperature swings experienced during operation, resulting in the accumulation of plastic strain. This builds up damage and results in bond degradation and eventual failure. The extent and rate of wire bond degradation depends on both the magnitude and duration of exposure to the operational and environmental temperature loads. Recent work has shown that thermally activated microstructural changes including recovery, recrystallization and grain growth can offset the damage accumulated during thermo mechanical fatigue under certain conditions [1]. Regrettably, commonly adopted physics-of-failure based models present consequential shortcomings, including their inability to correctly account for this thermally activated "damage removal" effect or other pertinent factors such as irregular loading profiles. When these factors are ignored, erroneous life prediction might result. This has been explained in detail by the authors in [2] which presented a review of the existing physics-of-failure models for wire bond interconnects and proposed the damage based crack propagation model to replace the usual cycle-dependent modeling methodology with a time domain representation.

This modeling methodology is intended to estimate the bonding interface damage condition at regular time intervals through a damage model which includes the effect of terms representing thermally activated processes on the bond degradation behavior. In addition, underlying factors which may vary for different materials and which influence the build-up of damage, such as stacking fault energy are also taken into account implicitly by the use of a representative work hardening term. Thus the impact of time-at-temperature and other rate sensitive processes on the bond degradation rate can be accurately represented.

Manuscript received April 7, 2014; revised August 27, 2014; accepted August 30, 2014. Date of publication September 4, 2014; date of current version December 2, 2014. This work was supported in part by the Innovative Electronics Manufacturing Research Centre (IeMRC) funded by the U.K. Engineering and Physical Sciences Research Council (EPSRC) through Research Grant EP/H03014X/1 and in part by the EPSRC National Centre for Power Electronics.

The authors are with the Department of Electrical and Electronic Engineering, Faculty of Engineering, University of Nottingham, Nottingham NG7 2RD, U.K. (e-mail: li.yang@nottingham.ac.uk; pearl.agyakwa@nottingham.ac.uk; mark.johnson@nottingham.ac.uk).

Color versions of one or more of the figures in this paper are available online at http://ieeexplore.ieee.org.

Digital Object Identifier 10.1109/TDMR.2014.2354739

II. Definition of the Damage Conceptual Model

In previous work, we presented compelling evidence for the simultaneous occurrence of strain hardening and softening in bond wires during temperature fluctuation, which was particularly pronounced for thermal cycling ranges with peak temperatures above 125 °C [1], [3], [4]. The occurrence of dynamic recovery and recrystallization during thermo mechanical fatigue also has been widely reported for isothermal fatigue conditions [5]–[7]. Since the observed grain coarsening and softening might be attributed to dislocation annihilation and a reversal of plastic strain [8], it was concluded by the authors in [2] that damage removal and damage accumulation occur in tandem during thermo mechanical cycling. In other words, the incremental damage (δD) is the combination of accumulated damage (δD^+) and damage removal (δD^-)

$$\delta D = \delta D^+ - \delta D^-. \tag{1}$$

Herein, we refer to "damage" as the extent of microstructural change. Microstructural mechanisms leading to the development of microvoids and microcracks are *damage accumulation processes*. These include for example the generation of crystallographic defects, perhaps bringing about localized grain misorientation. Processes which resolve this, by facilitating the annihilation, movement or rearrangement of dislocations and defects and thereby enhancing the material's ability to absorb more strain are therefore *damage removal processes*. Both damage accumulation and removal processes are assumed to occur simultaneously and are subject to spatial and temporal variation as a result of the applied loading conditions.

Under this definition, we propose that damage evolution, i.e., the microstructural change of the material, is associated with the development of dislocations and that it can be quantified by the plastic strain energy. Strain energy is generally

This work is licensed under a Creative Commons Attribution 3.0 License. For more information, see http://creativecommons.org/licenses/by/3.0/

represented by the strain energy density (U), defined as the strain energy per unit volume and it is composed of elastic energy (U_e) and plastic strain energy components (U_p):

$$U = \int \sigma d\varepsilon = U_e + U_p = \int \sigma(d\varepsilon_e + d\varepsilon_p) \tag{2}$$

where σ and $\varepsilon$are stress and strain; ε_e and ε_p are elastic and plastic strain respectively.

It is assumed that the accumulation of damage is attributable to irreversible changes in plastic strain energy. The elastic part, on the other hand, represents recoverable energy and does not contribute to the accumulation of damage.

The plastic work per unit volume is:

$$U_p = \int \sigma d\varepsilon_p. \tag{3}$$

The incremental damage accumulation term can be written in the form of plastic strain energy density as:

$$\delta D^+ = \sigma \delta \varepsilon_p. \tag{4}$$

In a loading event, it is assumed that the damage state and loading temperature determine the level of stress in the plastic region, i.e.,

$$\sigma = f(D, T). \tag{5}$$

Thereby the damage accumulation term is linked to strain energy density in terms of the pre-existing damage state and loading temperature as follows:

$$\delta D^+ = f(D, T)\delta \varepsilon_p. \tag{6}$$

Likewise, the rate of damage removal is determined by the existing damage state and loading temperature as well as the time at the temperature and can be represented as:

$$\delta D^- = \alpha(D, T)\delta t. \tag{7}$$

Therefore the incremental damage can be described by the following general expression:

$$\delta D = f(D, T)\delta \varepsilon_p - \alpha(D, T)\delta t. \tag{8}$$

This damage model accounts not only for the key physical process of work hardening during cyclic loading but also creep and stress relaxation over the monotonic loading regime. For example, in an isothermal stress relaxation process, in which strain remains constant i.e., $\delta \varepsilon_p = 0$; equation (8) becomes $\delta D = -\alpha(D, T)\delta t$ and so, depending on the temperature and damage state, the incremental damage will be negative which indicates a relaxation of stress or strain. And the expression for stress relaxation rate can be obtained by combining $\delta D = -\alpha(D, T)\delta t$ with equation (5):

$$\frac{d\sigma}{dt} = -\frac{\partial f(D, T)}{\partial D}\alpha(D, T). \tag{9}$$

Also under isothermal conditions, constant stress implies constant damage as indicated, so the change of damage δD is zero, i.e.,$0 = f(D, T)\delta \varepsilon_p - \alpha(D, T)\delta t$. The effective creep strain rate at constant stress is then given by:

$$\frac{d\varepsilon_p}{dt} = \frac{\alpha(D, T)}{f(D, T)}. \tag{10}$$

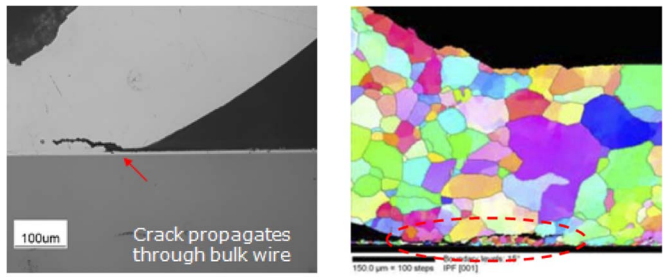

(a) (b)

Fig. 1. (a) An optical micrograph (b) An EBSD image [12] of a propagating crack in Al wire after thermal cycling.

Note that the assumption that the plastic stress level can be directly related to the damage state and temperature limits the applicability of this expression to conditions dominated by secondary creep, i.e., before the rupture phase.

So, by employing the above damage model, the wear-out physics of the wire bonds is represented in constitutive terms and the accumulation of "damage" is linked to a physically quantifiable property, namely the plastic strain energy density, which can be measured or extracted experimentally.

The constitutive functions of the damage model were proposed in [2]. In this manuscript, the functions and model parameters are calibrated by quantitatively linking the damage parameter D to experimentally derived strain energy density measurements.

III. Overview of the Lifetime Prediction Methodology Based on the Damage Model

In this section, a brief overview of the entire damage-based crack propagation model and consequential lifetime prediction is given to aid discussion although the details are described elsewhere [2].

Wire bond lift-off is predominantly the result of horizontal crack growth near bonding interface, attributable to stresses from the significant difference in thermal expansion behavior between the wire and chip material. It has been observed that cracks propagate within the bulk wire or just above the wire-metallization interface [9], [10]. Delamination may occur along the bonding interface between bonding pad and bond wire, and is usually due to inadequate surface cleaning or pre-existing oxide debris produced during bonding process [11]. However, under appropriate bonding conditions, a metallurgical bond is formed between the wire and metallization. Fig. 1 demonstrates a crack propagating through bulk wire after thermal cycling. In Fig. 1(b) [12], it can be seen that the crack initiated from interface and progressed through the wire along grain boundaries.

The same observation by Goehre *et al.* evidenced a crack path which did not advance along the bond interface but rather in the wire material approximately $10 \sim 20$ μm above the bond

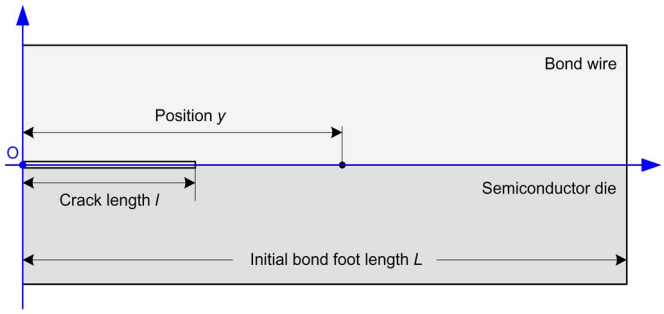

Fig. 2. A schematic representation of a wire bond.

interface [13]. It was discussed that the crack travels along the recrystallized grain boundaries in the wire material as this costs least efforts for crack propagation due to a prevailing hardening effect in the region between the crack and interface.

In this work, optimal bonding conditions are presumed thus "crack" refers to cracking in the metallurgical sense, rather than delaminating.

Fig. 2 shows a schematic diagram of a growing crack in a wire bond, for example as a result of repeated heating and cooling. A position at the bonding interface is represented by y, the distance from the origin O. L and l represent the original bond length and crack length respectively. The damage-based crack propagation model describes the evolution, in time and position, of a crack along an interface between two bonded materials with mismatched CTE (coefficient of thermal expansion) in which the damage condition in the wire material is estimated through the damage model (equation (8)). With a spatial plastic strain distribution function $g(y-l,\varepsilon)$ integrated into the damage accumulation term, which indicates the strain concentration factor at a position with respect to the crack tip along the bonding interface, the incremental damage at any point along the interface can be described by the differential model in the following expression:

$$\delta D(y,t) = f(D,T)\delta\varepsilon_{CTE}\cdot g(y-l) - \alpha(D,T)\delta t. \quad (11)$$

In this case, ε_{CTE} is the mismatched CTE induced strain in the wire material in the bonded condition.

The total interface damage (D_T) at each time instant (t) can be calculated by the integration of the damage for all the points along the interface from the crack tip

$$D_T(t) = \int_{y=l}^{y=L} D(y,t)dy. \quad (12)$$

Crack growth rate is a function of total damage and the rate of change of total damage, i.e.,

$$\frac{dl}{dt} = p(D_T) + q\left(\frac{dD_T}{dt}\right). \quad (13)$$

Thereby the remaining useful lifetime (RUL) of the wire bond interconnects can be estimated by

$$RUL = \frac{L-l}{L}. \quad (14)$$

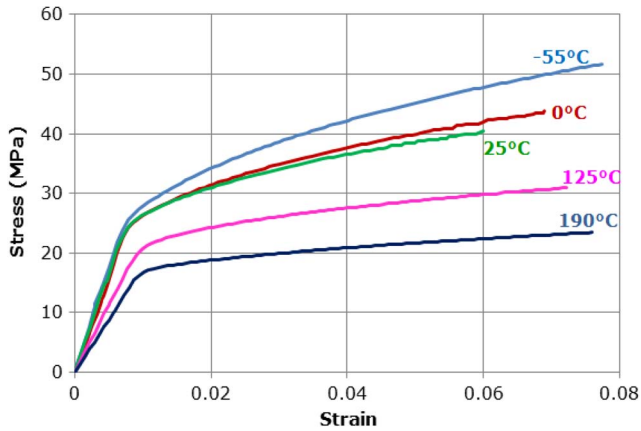

Fig. 3. Flow curves at different temperatures for 5 N 375 μm aluminum bond wires at strain rate of 0.0007/s.

IV. Development of the Damage Conceptual Model

In this new time-domain lifetime prediction methodology, development and calibration of the damage conceptual model (equation (8)) is paramount. This manuscript hereafter focuses on this aspect.

A. Evaluation of Plastic Strain Energy Density

Now that the concept of damage is linked to plastic strain energy, the first step is to extract the values of plastic strain energy density from tensile stress-strain curves in order to determine the constitutive functions of the damage model and calibrate the model parameters.

Isothermal, uniaxial tensile testing was carried out to evaluate the dynamic stress-strain response of bond wires used for power module interconnects. For the tests, 99.999% (5N) pure aluminum wire, 375 μm in diameter was cut into approximately 25 mm lengths. The samples were subsequently mounted onto paper tabs to minimize their handling while being clamped into position. The paper tabs provided means by which the samples could be more easily manipulated. Each wire was clamped into place with a fixed value of torque. Testing was performed on a Dynamic Mechanical Analyzer (DMA-Q800, TA Instruments) with a maximum load capacity of 18N, and displacement and force resolutions of 1 nm and 0.00001 N respectively. Isothermal uniaxial tensile tests were then performed at constant strain rate values ranging from of 1.7×10^{-6}/s to 7×10^{-4}/s and at temperatures ranging from -55 °C to 190 °C. The tensile tests were terminated at between 8% and 10% strain. Fig. 3 demonstrates the experimental stress-strain curves for strain rate of $\dot{\varepsilon} = 0.0007$/s at different temperatures.

The plastic strain energy absorbed to reach a strain of 6% is estimated for all the test conditions. The values of plastic strain energy density are plotted against temperature in Fig. 4. They show a clear linear relationship with regard to temperature at a constant strain rate which is demonstrated by the dashed trend lines.

B. Development of the Damage Model

1) Damage Accumulation Term: The work hardening part of a uniaxial stress-strain curve can be approximated with a

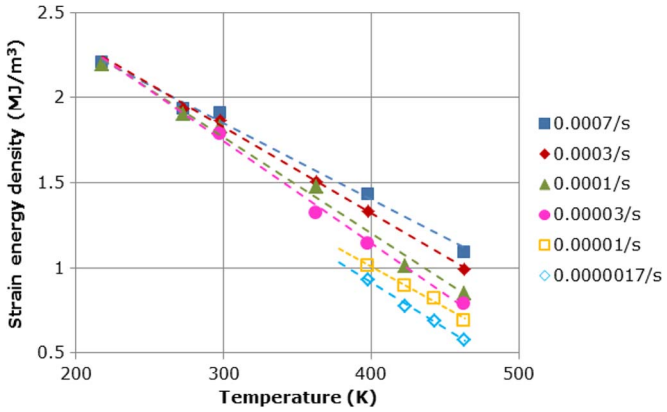

Fig. 4. Plastic strain energy density and linear trend lines against temperature derived from flow curves for 5 N 375 μm aluminum bond wires.

straight line that allows a linear work hardening function. Similarly, in view of the linear relationship between strain energy density and testing temperature shown in Fig. 4, the temperature dependent function can also be expressed by a linear function. Therefore the damage accumulation term is written as:

$$\delta D^{+} = [1 + \alpha_H \cdot \varepsilon_p] \cdot (\alpha_T - \beta_T \cdot T)\delta\varepsilon_p \tag{15}$$

where α_H is the work hardening constant; α_T and β_T are temperature hardening constants. It is expected that the strain hardening behavior is represented in terms of existing damage instead of strain. A relationship between strain and damage is therefore necessary.

Under low temperature, high strain rate testing condition, it can be assumed that damage accumulation is dominant in wire samples with negligible damage removal processes. Strain is approximately linear with stress in a work hardening curve:

$$\sigma = \frac{dD}{d\varepsilon} = b + a \cdot \varepsilon_p \tag{16}$$

where a and b are the slope of the work hardening line and yield point respectively.

Then a relationship between strain and damage is obtained.

$$\varepsilon_p = \frac{-b \pm \sqrt{b^2 + 2aD}}{a} \tag{17}$$

Replacing the strain ε_p in (15) with the damage expression in (17), we now have the differential damage accumulation model:

$$\delta D^{+} = \left[1 + \alpha_H \left(\frac{\sqrt{b^2 + 2aD} - b}{a}\right)\right] \cdot (\alpha_T - \beta_T \cdot T) \cdot \delta\varepsilon_p. \tag{18}$$

Equation (18) was implemented in MATLAB through explicit differentiation. Work hardening behavior based on damage condition in the material can be simulated by

$$\sigma = \frac{dD^{+}}{d\varepsilon_p} = \left[1 + \alpha_H \left(\frac{\sqrt{b^2 + 2aD} - b}{a}\right)\right] \cdot (\alpha_T - \beta_T \cdot T). \tag{19}$$

There are five parameters in equation (19), namely a, b, α_H, α_T and β_T. The values of b and a are determined by the stress-strain curve at -55 °C, $\dot{\varepsilon} = 0.0007/\text{s}$ as the lowest temperature point and fastest strain rate in the whole set of tensile test data.

TABLE I
THE VALUES OF MODEL PARAMETERS CALIBRATED BY STRESS-STRAIN CURVES WITH A STRAIN RATE OF 0.0007/s

a	b	α_H	α_T	β_T
329	29	20	26	0.036

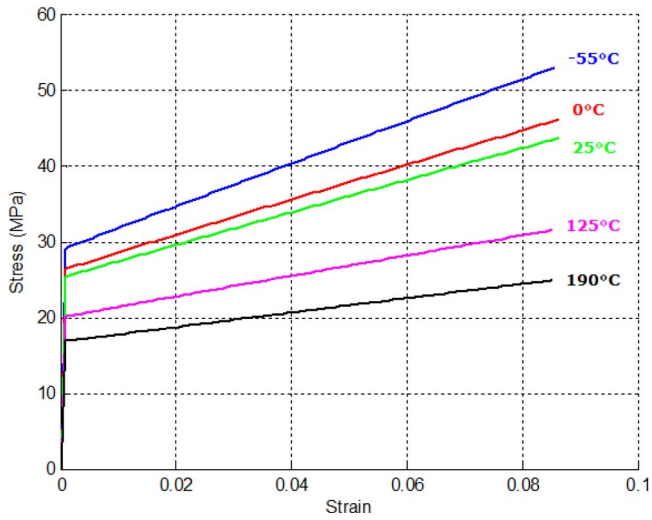

Fig. 5. Simulated work hardening curves with strain rate of 0.0007/s at different temperatures.

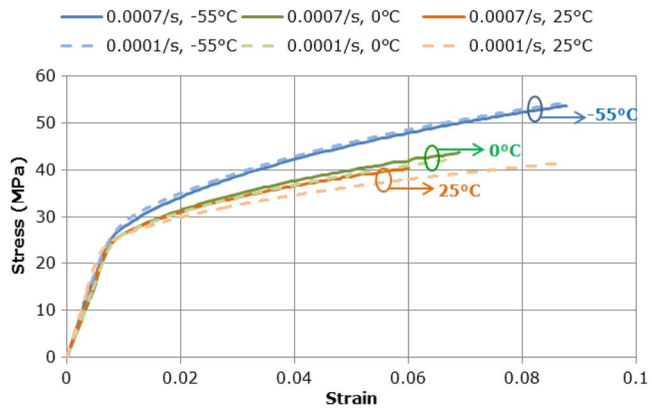

Fig. 6. Stress-strain curves for 5 N 375 μm Al wire at -55 °C, 0 °C, and 25 °C at strain rate of 0.0001/s and 0.0007/s.

The values of parameter α_H, α_T, and β_T are calibrated by fitting the slope of the work hardening stress-strain line as well as the yield point in a set of experimental stress-strain curves for the highest strain rate of $\dot{\varepsilon} = 0.0007/\text{s}$ at different temperatures (Fig. 3).

The values of these parameters are listed in Table I and the simulated work hardening curves based on the damage evolution corresponding to strain rate of $\dot{\varepsilon} = 0.0007/\text{s}$ at different temperatures are plotted in Fig. 5. Elastic deformation is recoverable so there is no damage accumulation and thus is not relevant to the damage model. Therefore the elastic part of the stress-strain curve is not included in this figure.

2) Damage Removal Term: Fig. 6 shows three sets of experimental stress-strain curves for 5 N 375 μm aluminum bond wires at the relatively low temperatures -55 °C, 0 °C, and

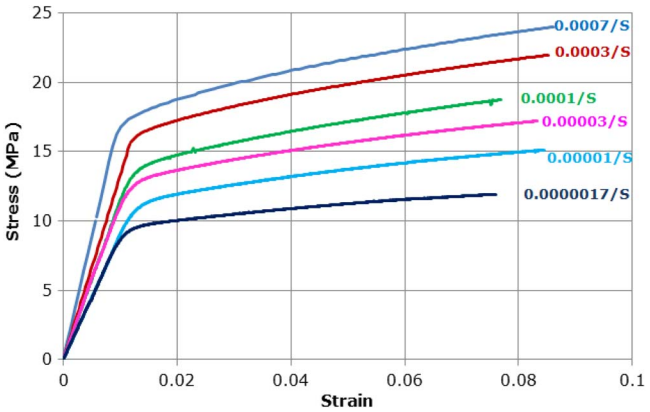

Fig. 7. Flow curves at 190 °C for 5 N 375 μm Al wire with different strain rates.

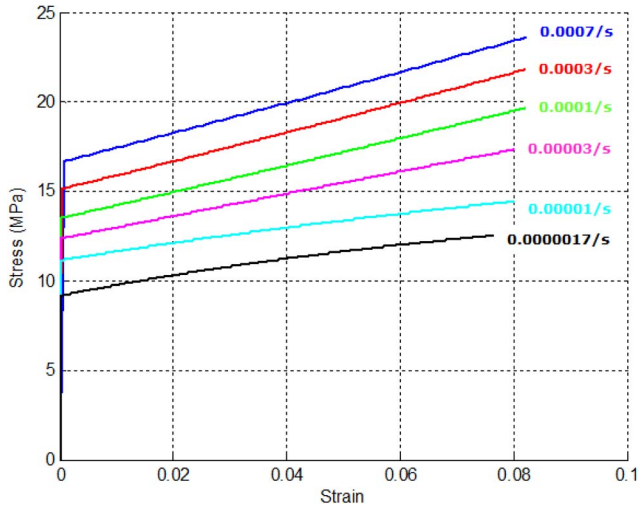

Fig. 8. Simulated work hardening curves at 190 °C with different strain rates.

25 °C at strain rates of 0.0001/s and 0.0007/s respectively. Curves corresponding to strain rate of 0.0007/s are marked with solid lines; those marked with dash lines correspond to strain rate of 0.0001/s.

It can be seen clearly that at −55 °C, the flow curves for the strain rate of 0.0007/s and 0.0001/s nearly overlap (Fig. 6). In the flow curves for 0 °C and 25 °C, the dispersion with regard to strain rate is slightly larger.

Fig. 7 illustrates the flow curves measured at 190 °C with strain rates ranging from $1.7 \times 10^{-6}/\text{s}$ to $7 \times 10^{-4}/\text{s}$.

In comparison, at temperature as high as 190 °C, the dispersion is much larger (Fig. 7).

Taken together, these results indicate that damage accumulation dominates with very little rate dependence at low temperatures but at high temperatures, time at temperature has a significant influence on thermally-activated damage removal effect.

Thus in the damage removal term (δD^-), the Arrhenius expression is used to reflect the dependence of the damage annihilation rate on temperature T, i.e.,

$$\delta D^- = \alpha(D,T)\delta t = D \cdot k_2' \, exp\left(-\frac{Q}{RT}\right)\delta t \qquad (20)$$

where Q is the activation energy, R is the gas constant, and k_2' is an annealing coefficient.

Now a complete damage model is achieved by combining the damage removal term (equation (20)) with the damage accumulation term (equation (18))

$$\delta D = \left[1 + \alpha_H \frac{\sqrt{b^2 + 2aD} - b}{a}\right] \cdot (\alpha_T - \beta_T \cdot T) \cdot \delta\varepsilon_p - D \cdot k_2' exp\left(-\frac{Q}{RT}\right)\delta t. \qquad (21)$$

Equation (21) was implemented in MATLAB through a time stepping model.

It needs to be noted that plastic strain energy density is accounted for by the damage accumulation term $\delta D^+ = \sigma\delta\varepsilon p$, however the level of damage and hence the stress-strain response is also affected by damage removal. Therefore, equation (21) is employed to evaluate the total amount of damage but the values of stress are extracted from equation (19), i.e., $\sigma = dD^+/d\varepsilon_p$.

In the simulation model, the annealing coefficient k_2' and activation energy Q influence the slope of the work hardening line and induce consequential change in strain energy density. The value of these two parameters can be calibrated by the set of experimental stress-strain curves for the highest temperature tested (190 °C) at different strain rates (Fig. 7), as these are most heavily influenced by thermally activated phenomena.

It can be seen from Fig. 7 that the yield point varies with respect to the different strain rates, suggesting different states of "initial damage." This is to be expected, as the effect of varying strain rate amounts essentially to varying the time at temperature. It therefore makes sense in the simulation model to set the initial damage to different values corresponding to the different yield points resulting from the different strain rates. Fig. 8 shows the simulated work hardening curves at 190 °C at different strain rates when k_2' and Q are set to 20 and 56 000 J/mol, respectively.

C. Evaluation of Accumulated Damage Under Isothermal Tension Loading Conditions

By way of verification of the calibrated damage model, equation (21) can now be used to evaluate the accumulated damage δD^+ for 6% strain, i.e., as per the strain energy density values calculated from the uniaxial tensile test data. The experimentally derived plastic strain energy density and the values of strain energy induced damage predicted by the model are listed in Table II together with values of relative errors. Agreement is generally better than 6% across the range of strain rates and temperatures with an average error of less than 3%, endorsing our approach to calibration. In just two cases ($\dot{\varepsilon} = 0.00003/\text{s}$, $T = 90$ °C; and $\dot{\varepsilon} = 0.00001/\text{s}$, $T = 125$ °C), the relative errors are around 10%. We suspect this may be due to the experiment error.

V. Conclusion and Further Work

The aim of the present work has been to develop and calibrate a constitutive damage model which forms the principal

TABLE II
COMPARISON OF EXPERIMENTAL VALUES OF STRAIN ENERGY DENSITY (MJ/m^3) AND SIMULATION OF DAMAGE (MJ/m^3)

Strain rate	Results \ T	218K	273K	298K	363K	398K	423K	443K	463K
0.0007/s	Experiment	2.205	1.937	1.912	—	1.429	—	—	1.094
	Simulation	2.247	1.986	1.870		1.429			1.158
	Relative error (%)	1.905	2.530	2.197		0			5.850
0.0003/s	Experiment	—	1.937	1.863	1.509	1.331	—	—	0.993
	Simulation		1.984	1.860	1.566	1.352			1.019
	Relative error (%)		2.426	0.161	3.777	1.578			2.618
0.0001/s	Experiment	2.193	1.904	1.828	1.475	—	1.012	—	0.851
	Simulation	2.242	1.979	1.838	1.527		1.012		0.899
	Relative error (%)	2.234	3.939	0.547	3.525		0		5.640
0.00003/s	Experiment	—	—	1.784	1.323	1.141	—	—	0.787
	Simulation			1.806	1.455	1.176			0.793
	Relative error (%)			1.233	9.977	3.067			0.762
0.00001/s	Experiment	—	—	—	—	1.010	0.895	0.821	0.689
	Simulation					1.112	0.902	0.820	0.686
	Relative error (%)					10.099	0.782	0.122	0.435
0.0000017/s	Experiment	—	—	—	—	0.929	0.774	0.689	0.575
	Simulation					0.954	0.817	0.705	0.571
	Relative error (%)					2.691	5.556	2.322	0.696

part of a recently proposed time-domain, damage-based crack propagation model for the lifetime prediction of wire bond interconnects.

The damage model is calibrated by quantitatively linking the damage parameter to plastic strain energy evaluated from flow curves which were obtained for pure aluminum (99.999%) wires by means of uniaxial tensile tests under various temperatures and strain rates. The constitutive material representation is determined by reference to the experimental stress-strain curves. The damage accumulation term is calibrated with the highest strain rate data and damage removal function, which reflects the influence of temperature and time on the accrued damage, is calibrated by the stress-strain data at the highest temperature with various strain rates. Then the whole constitutive damage model is verified by good agreement between values of damage accumulation and experimentally derived values of strain energy density under all testing conditions.

In the next step, this verified constitutive damage model will be applied in the crack propagation model to calibrate the crack propagation model against wire bond wear-out data collected from both active and passive thermal cycling experiments under different temperature profiles.

ACKNOWLEDGMENT

The authors wish to thank Dynex Semiconductors Ltd., for providing the bonded substrate tiles.

REFERENCES

[1] P. A. Agyakwa *et al.*, "Microstructural evolution of ultrasonic bonded high purity Al wire during extended range thermal cycling," *Microelectron. Reliab.*, vol. 51, no. 2, pp. 406–415, Feb. 2011.

[2] L. Yang, P. A. Agyakwa, and C. M. Johnson, "Physics-of-failure lifetime prediction models for wire bond interconnects in power electronic modules," *IEEE Trans. Device Mater. Rel.*, vol. 13, no. 1, pp. 9–17, Mar. 2013.

[3] P. A. Agyakwa *et al.*, "Anomalous reliability behaviour of 99.99% and 99.999% pure aluminium wire bonds under thermal cycling," in *Proc. 41st IMAPS*, Providence, RI, USA, 2008, pp. 658–665.

[4] C. Y. Yu, P. L. Sun, P. W. Kao, and C. P. Chang, "Evolution of microstructure during annealing of a severely deformed aluminium," *Mater. Sci. Eng.*, vol. 366, no. 2, pp. 310–317, Feb. 15, 2004.

[5] G. Khatibi *et al.*, "Accelerated mechanical fatigue testing and lifetime of interconnects in microelectronics," *Proc. Eng.*, vol. 2, no. 1, pp. 511–519, Apr. 2010.

[6] Y. Nakanishi, T. Fujii, S. Onaka, and M. Kato, "Low-cycle fatigue of ultrafine-grained aluminum at low temperatures," *Mater. Trans.*, vol. 52, no. 5, pp. 890–894, May 2011.

[7] H. W. Höppel, Z. M. Zhou, H. Mughrabi, and R. Z. Valiev, "Microstructural study of the parameters governing coarsening and cyclic softening in fatigued ultrafine-grained copper," *Philos. Mag. A*, vol. 82, no. 9, pp. 1781–1794, Jun. 2002.

[8] N. Murdeshwar and J. E. Krzanowski, "A microstructural study of dislocation substructures formed in metal foil substrates during ultrasonic wire bonding," *Metallurgical Mater. Trans. A*, vol. 28, no. 12, pp. 2663–2671, Dec. 1997.

[9] M. Ciappa and P. Malberti, "Plastic-strain of aluminum interconnects during pulsed operation of Igbt multichip modules," *Qual. Rel. Eng. Int.*, vol. 12, pp. 297–303, 1996.

[10] S. Ramminger, P. T Türkes, and G. Wachutka, "Crack mechanism in wire bonding joints," in *Proc. ESREF*, vol. 38, *Microelectron. Rel.*, Copenhagen, Denmark, Jun.–Aug. 1998, no. 6–8, pp. 1301–1305.

[11] W. S. Loh *et al.*, "Effect of bonding temperature, post-bond annealing and extended range thermal cycling on the reliability of al wire bonds," in *Proc. IMAPS Int. Conf. Exhib. High Temp. Electron.*, Albuquerque, NM, USA, May 12–15, 2008.

[12] Y. Yamada *et al.*, "Reliability of wire-bonding and solder joint for high temperature operation of power semiconductor device," *Microelectron. Rel.*, vol. 47, no. 12, pp. 2147–2151, Dec. 2007.

[13] J. Goehre, M.S.-R. , U. Geißler, and K.-D. Lang, "Interface degradation of al heavy wire bonds on power semiconductors during active power cycling measured by the shear test," in *Proc. CIPS*, Nuremberg, Germany, Mar. 16–18, 2010, pp. 1–6.

Authors' photographies and biographies not available at the time of publication.